



Article

# An AI-Driven Particle Filter Technology for Battery System State Estimation and RUL Prediction

**Mohamed Ahwiadi** and **Wilson Wang** \* 

Department of Mechanical and Mechatronics Engineering, Lakehead University, Thunder Bay, ON P7B 5E1, Canada; mahwiadi@lakeheadu.ca

\* Correspondence: [wwang3@lakeheadu.ca](mailto:wwang3@lakeheadu.ca)

**Abstract:** The increasing demand for reliable and safe Lithium-ion (Li-ion) batteries requires more accurate estimation of state of health (SOH) and remaining useful life (RUL) prediction. However, the inherent complexity and non-linear dynamics of Li-ion batteries present specific challenges to traditional methods of SOH modeling. Although particle filter (PF) techniques can handle nonlinear dynamics, they still face challenges, including particle degeneracy and loss of diversity, that reduce their ability to effectively model the nonlinear degradation mechanisms of batteries. To tackle these limitations, this paper presents a novel artificial intelligence-driven PF (AI-PF) technology for battery health modeling and prognosis. The main contributions of the AI-PF technique are as follows: (1) A novel dynamic sample degeneracy detection method is proposed to provide real-time assessment of particle weights so as to promptly identify degeneracy and improve computational efficiency. (2) An adaptive crossover and mutation strategy is proposed to reallocate low-weight particles and maintain particle diversity to improve modeling and RUL forecasting accuracy. The effectiveness of the AI-PF framework is validated through systematic evaluations carried out using benchmark models and well-recognized battery datasets.

**Keywords:** lithium-ion batteries; state of health estimation; remaining useful life prediction; AI-driven modeling; particle filter; crossover and mutation; sample degeneracy detection



**Citation:** Ahwiadi, M.; Wang, W. An AI-Driven Particle Filter Technology for Battery System State Estimation and RUL Prediction. *Batteries* **2024**, *10*, 437. <https://doi.org/10.3390/batteries10120437>

Academic Editors: Mona Faraji Niri, Truong Minh Ngoc Bui and Truong Quang Dinh

Received: 22 October 2024

Revised: 28 November 2024

Accepted: 6 December 2024

Published: 8 December 2024



**Copyright:** © 2024 by the authors. Licensee MDPI, Basel, Switzerland. This article is an open access article distributed under the terms and conditions of the Creative Commons Attribution (CC BY) license (<https://creativecommons.org/licenses/by/4.0/>).

## 1. Introduction

Lithium-ion (Li-ion) batteries are widely used in modern industries such as electric vehicles, renewable energy, and portable electronics due to their high energy density and efficiency [1,2]. However, Li-ion batteries experience natural degradation over time, which is characterized by capacity loss and increased impedance. This deterioration presents substantial challenges in maintaining optimal system performance and increases the risk of unexpected early system failures [3,4]. Therefore, it is critical to develop more accurate and reliable technology for monitoring the battery's state of health (SOH) and predicting its remaining useful life (RUL) to enhance operation safety and reliability.

Traditionally, two main approaches are applied to assess battery health and predict RUL: data-driven techniques and model-based methods [4,5]. Data-driven techniques, such as relevance vector machine, support vector machine, neural networks, fuzzy logic, and other machine learning algorithms, rely on historical data (e.g., voltage, current and impedance) to identify patterns and features of battery system to forecast its degradation trends and estimate the RUL [5–9]. While these techniques can perform well in controlled environments, they are usually inefficient to adapt battery performance under time-varying operating conditions such as temperature changes, load variations, and different cycling patterns [5,10,11]. Consequently, such limitations reduce the adaptability of classical data-driven techniques, particularly when predicting long-term degradation trends in dynamic environments [12].

In contrast, model-based methods offer several advantages in battery SOH prognosis over data-driven techniques, particularly in simulating the underlying physical

characteristics governing battery degradation [4,5]. These methods can infer unobservable system states, such as damage parameters and degradation indicators, which are critical for understanding the battery's SOH degradation processes [1,3,4]. Additionally, model-based methods can usually adapt to variations in operational environments, including fluctuations in temperature, load, and usage patterns, which make them more reliable in real-world applications [1,5]. By integrating uncertainty quantification into the estimates of model-based methods, they can provide more reliable state estimation and RUL predictions [5,11,13]. In general, model-based approaches utilize mathematical models and filtering techniques such as the Kalman filter (KF) and particle filter (PF) to track the evolution of battery SOH over time [5,13]. The accuracy of these filtering techniques depends on the identification of key model parameters, which is crucial for these diagnostic models to accurately analyze the battery SOH and predict the RUL [14,15].

While the KF technique can provide an adequate solution to model linear-Gaussian estimation problems, it faces challenges to be applied for system modeling of nonlinear or non-Gaussian dynamics, such as Li-ion batteries [3,4,16]. PF techniques, on the other hand, represent the posterior probability density function (PDF) through a set of weighted particles [3,13], and can model nonlinear and non-Gaussian system characteristics in battery systems for system SOH monitoring [4,13], fault detection [17], and prognostics [3]. For example, ref. [18] used PFs to estimate parameters in an exponential growth model that describes electrolyte and charge transfer resistances to predict the RUL of Li-ion batteries. An empirical model incorporating Coulombic efficiency was suggested in [19] to estimate PF model parameters and to predict battery behaviors and degradation patterns. The authors of [20] compared PF with other estimation methods such as the unscented KF and nonlinear least squares for Li-ion battery prognosis. The findings indicated that PFs perform better, especially under nonlinear degradation conditions. PFs were applied in [21] to estimate parameters in Brownian motion degradation models for SOH estimation and RUL prediction. Furthermore, a PF prognostic model was proposed in [22] by incorporating discharge rate dependency for battery SOH monitoring under time-varying loads and discharge operating conditions.

Despite these advantages over KFs, PFs have some limitations in applications, such as sample degeneracy. Sample degeneracy is a problem in which only a few particles have high weights and can contribute to the estimate, while most particles have very low weights without clear contributions to system state estimation [17,23]. This problem can lead to sample impoverishment during the resampling process, in which high-weight particles are duplicated and low-weight particles are discarded, leading to particle diversity degradation [23]. This limitation becomes more problematic over extended time horizons, leading to reduced accuracy in state estimation and RUL predictions [24].

Several improved PF techniques were proposed to address these limitations in nonlinear system modeling and SOH estimation. A common strategy is to optimize the proposal distribution to make particles reflect the true posterior distribution. For instance, a Gaussian PF was introduced in [25] to approximate the posterior distribution and reduce the mismatch between the proposal and the true posterior. An auxiliary PF was suggested in [26] to incorporate an auxiliary variable to guide particle selection for RUL estimation. An unscented PF (UPF) was suggested in [27] by combining the unscented KF with PF to increase particle diversity and improve particle generation. Additionally, a spherical cubature PF was suggested in [28] to propagate particles in system modeling so as to reduce sample degeneracy. In the above methods, optimizing the proposal distribution typically requires more particles in processing, which increases computational complexity [24]. Moreover, some of these PF techniques, like the Gaussian PFs, are highly sensitive to the accuracy of the system and observation models, which limits their robustness and can result in reducing estimation accuracy [23].

Another approach to tackling sample degeneracy focuses on smoothing the posterior PDF density to improve the diversity of particles using certain regularization algorithms. For example, a regularized PF presented in [29] employs kernel density estimation to

spread particles more uniformly in the system space to maintain particle diversity. An extension to this method is the regularized auxiliary PF [30], which applies a regularization step to enhance particle diversity. Similarly, an adaptive kernel auxiliary PF was presented in [31] to adjust the kernel bandwidth to improve the posterior distribution. The Rao-Blackwellized PF was integrated with a mixture regularization technique in [32] to enhance importance sampling. Although regularization-related methods could improve particle diversity, they need continuous resampling and kernel adjustments, which may not be able to capture sharp changes or complex behaviors in posterior distributions [23].

Recent research has explored integrating AI into PF frameworks to optimize particle distribution and address sample degeneracy and impoverishment. These methods employ mutation strategies, swarm intelligence, and hybrid approaches to enhance state estimation and improve RUL prediction accuracy. For instance, a mutated PF was proposed in [4], which uses a mutation-based mechanism to explore the posterior PDF. This approach aims to achieve a better posterior distribution and improve battery state estimation and RUL prediction. Similarly, an intelligent PF was suggested in [33], which incorporates genetic algorithm operators to mitigate particle impoverishment. Another advancement was the use of the adaptive genetic algorithm PF in [34], which adjusts genetic operators to mitigate sample impoverishment and enhance estimation accuracy in nonlinear systems. Swarm intelligence techniques were also applied for advanced PF applications. For example, an artificial fish swarm PF technique was suggested in [35] to combine data-driven and model-based approaches to mimic fish foraging and clustering behaviors to explore the state space so as to improve the RUL prediction of Li-ion batteries. A quantum particle swarm optimization PF was proposed in [36], which uses quantum-inspired principles to achieve global search efficiency and identify high-likelihood regions in the state space. Another swarm-inspired technique was the firefly algorithm for PF optimization [37], which adopts an intelligent resampling strategy to locate high-likelihood regions so as to enhance particle diversity.

Hybrid approaches of PF frameworks are also recognized by integrating machine learning and fuzzy logic. For instance, a neural-network-assisted PF was suggested in [38], which uses machine learning models to capture battery degradation trends while dynamically fine-tuning model parameters. A hybrid PF with radial basis function neural networks was proposed in [39] to train the neural network in real time. Additionally, a T-S fuzzy model PF was developed in [40] to employ fuzzy logic and clustering to address non-Gaussian noise and nonlinear dynamics using an importance density function. While these AI-driven methods could improve PF performance to some extent in addressing particle degeneracy and enhancing state estimation, they still face notable limitations. For example, overfitting in parameter optimization remains a common issue, especially in approaches that integrate machine learning models [41–43]. Additionally, many of these methods are sensitive to noise, especially under high noise conditions or rapidly changing system dynamics, such as those in Li-ion batteries [5,14]. Computational complexity is another significant challenge, as swarm intelligence techniques and hybrid approaches are often complex in algorithms, which take more computation workload and limit their suitability for real-time monitoring applications [20]. Furthermore, the reliance on normalized particle weights to identify and process low-weight particles can lead to degraded estimation accuracy when particles cluster in low-likelihood regions [24]. These challenges emphasize the need for further research to develop adaptive, noise-resilient, and computationally efficient AI-PF methods for more accurate battery SOH monitoring and RUL prediction.

To address this challenge, the objective of this work is to develop a novel AI-driven PF (AI-PF) framework for more accurate estimation of battery SOH and RUL predictions. The contributions of the AI-PF technology are as follows: (1) A novel sample degeneracy detection method is proposed to assess particle weight distribution. Its purpose is to monitor the quality of the particle set in real time and promptly identify the onset of degeneracy. Unlike traditional PF methods that apply corrective measures to all particles at every iteration, this approach selectively targets degeneracy only when necessary so as

to enhance computational efficiency. (2) An enhanced crossover and mutation technique is proposed to reallocate identified low-weight particles to high-likelihood areas using an intelligent particle manipulation strategy to mitigate sample degeneracy and optimize particle diversity. The suggested crossover strategy can exchange information between high-weight particles to guide low-weight particles toward high-likelihood regions. Meanwhile, a novel adaptive mutation strength is used to better exploit high-likelihood regions and improve the modeling convergence.

The remainder of this paper is organized as follows: Section 2 presents the proposed AI-PT technique including the sample degeneracy detection method and enhanced crossover and mutation approach. Section 3 demonstrates the performance of the proposed AI-PT technique through simulation tests.

## 2. The Proposed AI-PF Technology

To tackle the inherent limitations of PF, this research introduces a novel AI-PF technology, in which the AI-PF leverages AI to optimize particle distribution so as to mitigate sample degeneracy and particle impoverishment. First, a brief review of standard PF will be presented in this section to provide context for the proposed technology, followed by the proposed sample degeneracy detection, and enhanced crossover and mutation method of the AI-PF technology.

### 2.1. Overview of the PF

PF is a class of sequential Monte Carlo methods for estimating the states of dynamic systems that are nonlinear and non-Gaussian [16], which represent the posterior distribution of a system's state through a group of weighted particles [24]. The fundamental principle of PF involves recursively propagating and updating a set of particles over time to approximate the posterior distribution of the system's state [17]. In a dynamic system, the state  $x_k$  at the time step  $k$  evolves according to a state transition function as in Equation (1):

$$x_k = f(x_{k-1}, u_{k-1}) \quad (1)$$

where  $f(\cdot)$  represents the state transition function of the dynamic system;  $u_k$  denotes the process noise, typically modeled as a zero-mean white noise sequence.

The observations  $y_k$  are affected by measurement noise  $v_k$  linked to the hidden state  $x_k$  such that:

$$y_k = h(x_k, v_k) \quad (2)$$

where  $h(\cdot)$  is the measurement function mapping the state space to the observation space. The posterior PDF,  $p(x_k|y_{1:k})$ , represents the probability of the state  $x_k$  given all observations up to time  $k$ . The PF approximates this posterior PDF by using a set of  $N$  weighted particles  $\{x_k^i, q_k^i\}_{i=1}^N$ , where  $x_k^i$  is the  $i$ -th particle at time step  $k$ , and  $q_k^i$  is its corresponding weight. Consequently, the posterior density at time  $k$  is estimated as follows:

$$p(x_k|y_{1:k}) \approx \sum_{i=1}^N q_k^i \delta(x_k - x_k^i) \quad (3)$$

where  $\delta$  is the Dirac delta function [17]. The weights  $q_k^i$  are updated recursively using the principle of importance sampling, with particles drawn from a proposal distribution  $q(x_k|x_{0:k-1}, y_{1:k})$ , or as follows:

$$q_k^i \propto q_{k-1}^i \frac{p(y_k|x_k^i)p(x_k^i|x_{k-1}^i)}{q(x_k^i|x_{0:k-1}^i, y_k)} \quad (4)$$

The weights are then normalized to ensure that the PF represents the posterior distribution:

$$\tilde{q}_k^i = \frac{q_k^i}{\sum_{j=1}^N q_k^j} \quad (5)$$

As discussed in the Introduction, as the PF iterates and propagates its particles, sample degeneracy may occur when most particles carry negligible weights, but only a few particles significantly contribute to the approximation of the posterior PDF. As a result, the particle set becomes less representative of the actual state of the system. The severity of sample degeneracy can be measured by the effective sample size (ESS) such that  $N_{ess}$  in Equation (6). This metric provides an estimate of the number of particles that effectively contribute to the state estimation [17], which can be calculated at each time step  $k$  as follows:

$$N_{ess} = \frac{1}{\sum_{i=1}^N (\tilde{q}_k^i)^2} \quad (6)$$

where  $N$  is the total number of particles. If  $N_{ess} \in [1, N]$  is close to  $N$ , the particle weights are nearly uniform or all particles contribute equally to the estimation. Otherwise, a smaller  $N_{ess}$  indicates that only a few particles have significant weights while the other particles have small contributions to the estimation process (severe degeneracy), as illustrated in Figure 1.

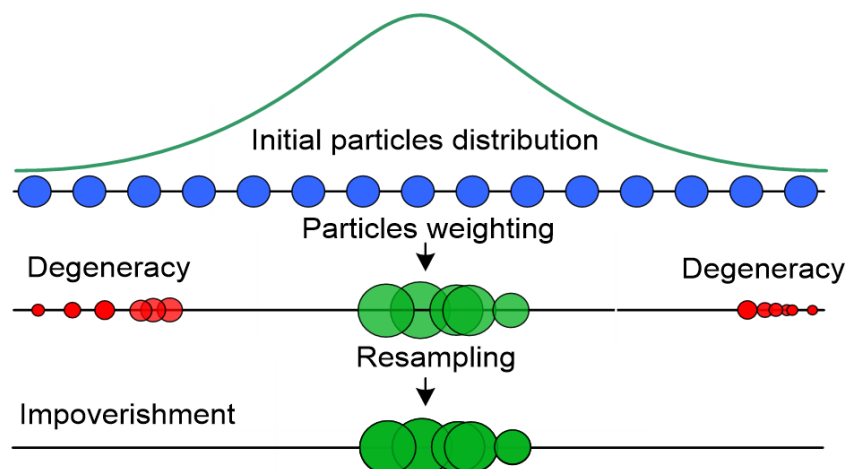


**Figure 1.** The impact of resampling on particle diversity, leading to sample impoverishment.

The resampling step method can be used to mitigate the sample [16,17] by replicating particles with higher weights and discarding those with lower weights. This process, however, can generate another problem known as sample impoverishment [23] when the diversity of the particle set decreases, as illustrated in Figure 1. Both particle degeneracy and impoverishment prevent the PF from thoroughly exploring the state space, which leads to less accurate state estimates.

With the limitations of PF in mind, the following subsections will introduce the developed AI-PF technology, including the proposed sample degeneracy detection method, and the novel crossover and mutation technique.

## 2.2. The Proposed Sample Degeneracy Detection Method

The proposed sample degeneracy detection (SDD) method will detect sample degeneracy using an adaptive weight threshold to recognize the low-weight particles that could contribute to degeneracy. Unlike conventional PF methods, which typically apply corrective measures at every iteration, the proposed SDD method continuously monitors

the quality of the particles during the filtering process to provide timely detection of sample degeneracy. The quality of particles at each iteration  $k$  is estimated by a quality measure  $Q_k$ :

$$Q_k = \frac{(\sum_{i=1}^N q_i^{(k)})^2}{\sum_{i=1}^N (q_i^{(k)})^2} \quad (7)$$

where  $q_i^{(k)}$  is the particle's unnormalized weights; and  $N$  is number of particles. The quality index  $Q_k$  reaches its maximum value  $N$ , when all particles are concentrated in the high-likelihood region, indicating no sample degeneracy. Conversely, a lower value of  $Q_k$  denotes that fewer particles carry significant weights while most contribute minimally to the overall estimate, which indicates a higher degree of degeneracy within the particle set. The proposed SDD method applies an adaptive threshold  $\tau_k$  to identify low-weight particles that degrade the overall quality of the particles and require corrective actions:

$$\tau_k = \begin{cases} 0.1 \times \max(q_i^k), & \text{if } Q_k < 0.5N \\ 0.05 \times \max(q_i^k), & \text{if } Q_k \geq 0.5N \end{cases} \quad (8)$$

This adaptive threshold  $\tau_k$  is fine-tuned according to the quality of the particle set. The condition  $Q_k < 0.5N$  is selected based on the consideration that significant sample degeneracy could occur when the effective sample size drops below half the total number of particles. In such scenarios, it is necessary to apply a higher threshold of  $0.1 \times \max(q_i^k)$  to restore larger low-weight particles to balance the particle distribution. Conversely, if  $Q_k \geq 0.5N$ , a well-distributed particle set, has low degeneracy, then a lower threshold of  $0.05 \times \max(q_i^k)$  can be used to make finer adjustments. The higher threshold can make more effective corrective action during high-degeneracy phases, while a lower threshold can be used to reduce adjustments during stable phases. This adaptive approach aims to maintain the overall quality of the particle set while avoiding unnecessary overhead. Figure 2 illustrates these two adjustment scenarios with a higher threshold and lower threshold conditions.

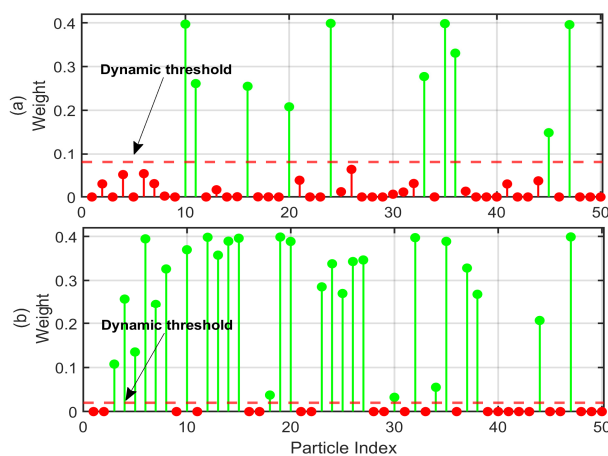


**Figure 2.** Illustration of the adaptive thresholds under two scenarios: (a) high sample degeneracy with a higher dynamic threshold; (b) low sample degeneracy with a lower threshold.

Once the low-weight particles are recognized, they will be further processed by using the proposed crossover and mutation technique as described in the next subsection.

### 2.3. The Proposed Crossover and Mutation Technique

The proposed crossover and mutation technique represents a key innovation within the AI-PF framework. Inspired by genetic algorithms in machine learning, this technique is designed to selectively relocate the recognized low-weight particles to higher-likelihood regions in the state space. This is to ensure a more accurate and better representation of the

posterior distribution so as to mitigate sample degeneracy. The crossover operation will facilitate the exchange of information between high-weight particles, while the mutation process will explore underrepresented regions of the state space.

### 2.3.1. The Proposed Crossover Strategy

The suggested crossover strategy aims to facilitate the exchange of information among high-weight particles in the particle set. For each low-weight particle identified through the SDD method as specified earlier, the crossover operation begins by randomly selecting two parent particles from the higher-weight particles that are usually located in high-likelihood regions. These particles are ideal candidates for guiding the recognized low-weight particles toward high-likelihood regions. If  $x_i$  is the  $i$ -th particle at time step  $k$  with a weight  $q_i$ , for simplicity, the parent particles with indices  $I$  and  $J$  are selected from higher-likelihood regions so that their respective weights  $q_I$  and  $q_J$  are among the highest weights. As illustrated in Figure 3, this parent selection strategy is to ensure that the crossover operation primarily involves particles that contribute more significantly to the posterior distribution.

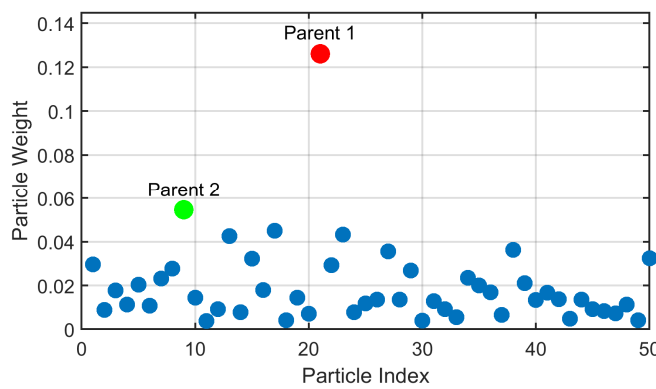


**Figure 3.** These two highest-weight particles are selected as parents for the crossover operation.

Once the parent particles are selected, the proposed crossover operation is to produce new particles that inherit characteristics from higher-weight parent particles so as to enhance the diversity and accuracy of the particle set. The new particle  $x_i^{new}$  is created as follows:

$$x_i^{new} = \alpha \cdot x_I + (1 - \alpha) \cdot x_J \quad (9)$$

where  $\alpha \in [0, 1]$  is the crossover coefficient that represents the contribution of each parent to the new particle;  $x_I$  and  $x_J$  denote the states of the selected two parent particles on the current particle set. In this crossover operation,  $\alpha$  is randomly selected over  $[0, 1]$  during each iteration. This randomness allows  $\alpha$  to vary naturally so as to ensure diverse contributions from the parent particles. This variability can prevent premature convergence and promote particle diversity without requiring additional computations. While  $\alpha$  is not explicitly adaptive, its random selection introduces an adaptive-like behavior that allows the crossover operation to balance computational efficiency and particle diversity effectively.

This crossover operation in Equation (9) can exchange information between high-weight particles and facilitate the relocation of identified low-weight particles to more favorable regions of the state space. The crossover coefficient  $\alpha$  can enable the particle set to avoid premature convergence and to maintain diversity. When  $\alpha$  is closer to 1, the new particle's state will be more similar to  $x_I$ ; otherwise, when  $\alpha$  is closer to 0, it is more similar to  $x_J$ . Figure 4 illustrates how different values of  $\alpha$  generate different new particles from both parent particles.

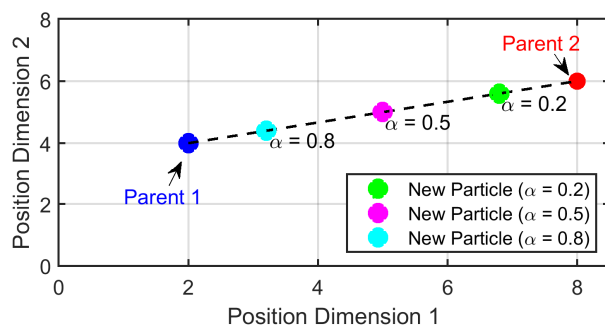


**Figure 4.** Crossover operation with different  $\alpha$  values, showing new particle generation.

### 2.3.2. The Proposed Mutation Strategy

Following the crossover operation, the mutation process will introduce controlled randomness to the new particles so as to explore the state space more effectively. Another purpose is to prevent the PF from prematurely converging to suboptimal solutions so that the PF remains responsive to changes in the system dynamics.

In the proposed mutation approach, an adaptive mutation strength  $\sigma_k$  is introduced in the following equation:

$$\sigma_k = \sqrt{u_k} \cdot \left( \frac{N - Q_k}{N} + 1 \right) \quad (10)$$

where  $Q_k$  is the quality of the particle set at the current time step  $k$ , which is determined from Equation (7);  $u_k$  is the process noise covariance, which determines the level of inherent randomness in the system;  $N$  is the number of particles.

This adaptive  $\sigma_k$  works to balance between exploration of the state space and exploitation of known high-likelihood regions. When sample degeneracy is high (i.e.,  $Q_k$  is low), a larger mutation strength  $\sigma_k$  is applied to explore a broader range of the state space to prevent the particles from concentrating in low-likelihood regions. Conversely, when the particle set is well distributed (i.e.,  $Q_k$  is high with a lower level of degeneracy), a smaller mutation strength  $\sigma_k$  can be used to make finer adjustments to the particle positions. This balance between exploration and exploitation can maintain a better and more diverse representation of the posterior distribution. The proposed mutation operation can be performed as follows:

$$x_i^{mutated} = x_i^{new} + \sigma_k \cdot \eta \quad (11)$$

where  $x_i^{mutated}$  is the mutated particle;  $x_i^{new}$  is the particle generated by the crossover operation; and  $\eta \in [0, 1]$  is a random number.

By adaptively adjusting the mutation strength  $\sigma_k$ , the proposed mutation strategy makes the PF responsive to varying system conditions within the state space. This adaptability is important in dynamic systems such as Li-ion batteries, whose true states may change with variable operating conditions. The proposed adaptive mutation can also reduce computational costs by limiting unnecessary mutation operations as used in the available mutation methods.

After the mutation, the newly mutated particle is integrated into the particle set, replacing the identified low-weight particle. In the developed AI-PF technology, the proposed crossover and mutation strategies will be integrated to maintain a better and diverse particle set to improve state estimation. Figure 5 illustrates the effect of particle distributions with and without using the proposed crossover and mutation technique. In Figure 5a, sample degeneracy is present; many particles have very low weights, which indicates a poor representation of the posterior distribution. After applying the proposed enhanced crossover and mutation technique, Figure 5b shows a more balanced distribution of particle weights in higher-likelihood areas. Thus, the enhanced crossover and mutation technique in the AI-PF technology can mitigate sample degeneracy and improve the state estimation accuracy.

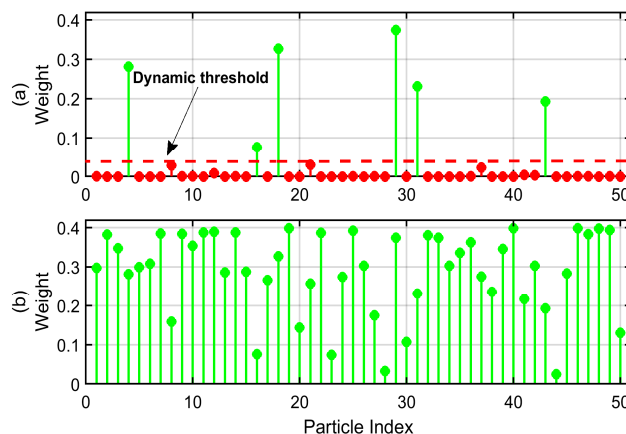


**Figure 5.** Comparison of particle distributions in two scenarios: (a) presence of sample degeneracy; (b) improved distribution after applying the proposed crossover and mutation technique.

### 3. Simulation Results and Performance Evaluation

The effectiveness of the proposed AI-PF technology will be evaluated in this section through extensive simulation tests using widely accepted benchmark models and battery datasets.

#### 3.1. Evaluation Using a Benchmark Model

The effectiveness of the proposed AI-PF technique in addressing sample degeneracy and impoverishment is examined using a benchmark model. It is a commonly used model in this research field as a test function, which has properties of nonlinear, periodic, and stochastic elements [4,16,17]. The benchmark model's state and measurement equations are defined as follows:

$$x_k = \frac{1}{2}x_{k-1} + \frac{25x_{k-1}}{1+x_{k-1}^2} + 8 \cos [1.2(k-1)] + u_k \quad (12)$$

$$y_k = \frac{1}{20}x_k^2 + v_k \quad (13)$$

where  $x_0$  represents the initial state;  $k$  is the number of time step; and  $v_k$  is the measurement noise variance.

To validate the performance of the proposed AI-PF, its results will be compared against well-known PF techniques such as sampling importance resampling PF (SIR-PF) [17], regularized PF (RPF) [29], unscented PF (UPF) [27], and mutated PF (MPF) [4]. The tests are conducted using MATLAB R2018b.

##### (1) Assessment of system state estimation:

During this analysis, the proposed AI-PF technique is employed to estimate the system state, specifically on mitigating sample degeneracy and impoverishment. The accuracy of estimation is measured by calculating the root-mean-square error (RMSE) between the estimated and actual states over 50 simulation runs. The test conditions are selected as follows: the process noise variance  $u = 10$ ; initial state  $x_0 = 0.1$ , the number of time steps  $k = 50$ ; and the measurement noise variance  $v = 1$ . The evaluation explores various particle counts:  $N = 15, 30, 45, 60$ , and  $75$ . Tables 1 and 2 provide comprehensive overviews of performance evaluation of the associated techniques with respect to estimation accuracy and consistency among different test conditions. Table 1 indicates that the proposed AI-PF consistently achieves the lowest RMSE across all tested particle numbers, which can demonstrate its enhanced estimation accuracy and reliability against sample degeneracy and impoverishment. Generally, as particle number increases, the RMSE values decrease; however, the proposed AI-PF demonstrates the most significant reduction in RMSE, due to its more efficient utilization of particles to capture system dynamics. For example, with

only 15 particles, the RMSE of AI-PF is 6.622, which is approximately 18%, lower than the SIR-PF, and around 8%, 15%, and 7% lower than the RPF, UPF, and MPF, respectively. When more particles (e.g.,  $N = 75$ ) are used, the AI-PF has better performance with an RMSE of 3.756, approximately 33% lower than the SIR-PF, 24% lower than both the RPF and UPF, and 17% lower than the MPF.

**Table 1.** Average RMSE of the related PF methods across different particle counts over 50 simulation runs.

Particle Counts	SIR-PF	RPF	UPF	MPF	AI-PF
15	8.117	7.221	7.843	7.094	6.622
30	6.696	6.181	6.516	6.066	5.497
45	5.997	5.579	6.076	5.559	4.636
60	5.294	5.178	5.320	5.022	4.199
75	5.121	4.947	4.901	4.552	3.756

**Table 2.** Average standard deviations of RMSE using different particles over 50 simulation runs.

Particle Counts	SIR-PF	RPF	UPF	MPF	AI-PF
15	1.745	1.391	1.963	1.822	1.047
30	1.696	1.468	1.430	1.430	0.656
45	1.171	0.920	0.993	0.811	0.431
60	1.029	0.577	0.757	0.746	0.449
75	0.585	0.586	0.410	0.451	0.352

Table 2 provides further evaluation of the related PF methods in terms of the averaged standard deviation of the RMSE to assess the consistency and robustness of the related methods. A lower standard deviation indicates better stability and robustness, which are essential for practical state estimation in Li-ion batteries. The results indicate that the AI-PF consistently shows the lowest standard deviation of RMSE across all particle number counts compared to other methods. For instance, with 15 particles, the AI-PF achieves a standard deviation of 1.047, approximately 40%, 24%, 46%, and 42% lower than the SIR-PF, RPF, UPF, and MPF, respectively. This demonstrates that the AI-PF can provide satisfactory performance even using fewer particles.

Figure 6 illustrates the performance of the PF techniques over 50 random runs with  $N = 45$  particles. The solid red line represents the actual system states, while each blue line represents the estimated states for an individual run. When the blue lines are closer to the red line, it indicates a significant reduction in estimation errors. Conversely, greater variability among the blue lines presents lower accuracy and robustness. It can be seen that the proposed AI-PF has adequate adaptive capability to adjust particle positions using its enhanced crossover and mutation techniques. It can focus on high-probability regions of the state space, and achieve optimal performance using the available particles. In contrast, the SIR-PF often suffers from sample impoverishment, especially using fewer particles, because the resampling process reduces particle diversity. Although the RPF and UPF offer some reasonable performance through the use of regularization and unscented transformation, they still cannot accurately represent the true posterior distribution in non-linear and complex state spaces. The regulation of the RPF may fail to balance smoothing with maintaining crucial details in the posterior distribution, while the UPF relies on Gaussian assumptions, which can misrepresent highly non-Gaussian distributions. Although the MPF can provide performance improvement by enhancing diversity, it relies on normalized particle weights to identify high-likelihood areas within the posterior space, which may cause the MPF to become trapped in local optima, particularly in non-linear and complex state spaces. These problems can limit the related PF techniques to effectively track the system dynamics.

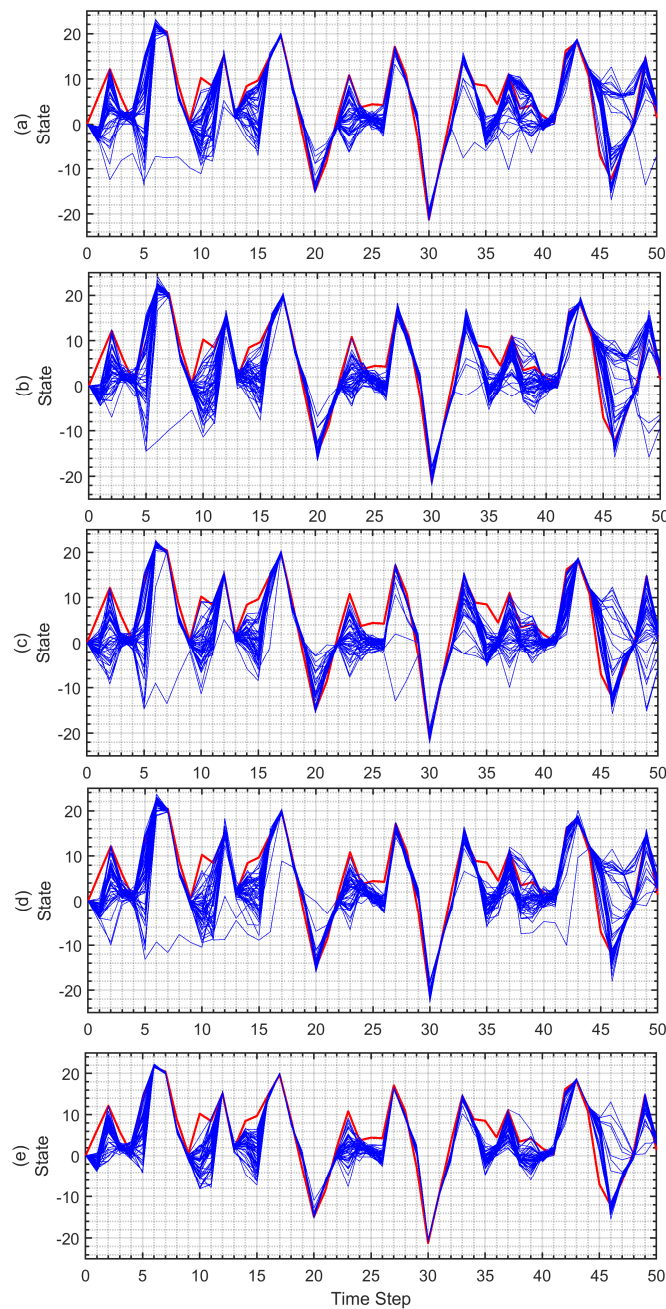


**Figure 6.** Comparison of performance using the respective PF techniques, including (a) SIR-PF, (b) RPF, (c) UPF, (d) MPF, and (e) AI-PF. The real states are represented by solid red line, and the estimated states are shown in blue lines over 50 runs.

## (2) Performance analysis under different noise conditions:

In this evaluation, the performance of the PF techniques is analyzed under different noise levels to assess their ability to handle sample degeneracy as noise can exacerbate degeneracy and degrade state estimation accuracy [24]. The tests are undertaken under different levels of process noise variances  $u = 5, 15, 25, 35, 45$ . Table 3 summarizes the average RMSE of the related PF methods over 100 simulation runs. Notably, the proposed AI-PF can achieve the lowest RMSE values across all noise levels, which demonstrates its robustness to maintain accurate state estimation even as noise increases. For instance, at a process noise variance of  $u = 5$ , the AI-PF has an RMSE of 4.467, approximately 20% lower than the SIR-PF and RPF, and 16% lower than the UPF and MPF. As the noise variance increases to 45, the AI-PF still has the lowest RMSE with an RMSE of 6.741, which is about

14%, 14%, 28% and 11% lower than the SIR-PF, RPF, UPF, and MPF, respectively. This is because, in the proposed AI-PF, the proposed sample degeneracy detection method can continuously monitor the quality of the particles and perform corrective actions using the suggested crossover and mutation techniques. These adjustments enable the AI-PF to effectively explore high-probability regions of the state space to maintain particle diversity and prevent sample degeneracy. In contrast, other PF methods exhibit higher RMSE values as noise increases; their working mechanisms could not properly represent the posterior distribution under high-noise conditions.

**Table 3.** Average RMSE under different process noise variances over 100 simulation runs.

Process Noise Variance	SIR-PF	RPF	UPF	MPF	AI-PF
5	5.614	5.612	5.351	5.363	4.467
15	5.882	5.526	6.373	5.463	5.059
25	7.460	6.719	7.624	6.613	6.212
35	8.120	8.090	9.058	8.221	6.452
45	7.736	7.757	9.554	7.598	6.741

Figure 7 shows the box plots representing the RMSE distributions across 100 runs with  $N = 40$  particles for each PF method under process noise variances of 5, 25, and 45. It is clear that the AI-PF has the lowest median RMSE with the shortest spread area (i.e., smallest error), which indicates better performance compared to other PF methods. In contrast, the other PF methods display wider spreads in their RMSE distributions, which reflect greater variations in estimation under noise. This adaptive capability of the AI-PF can make it more suitable for state estimation under varying noise conditions.

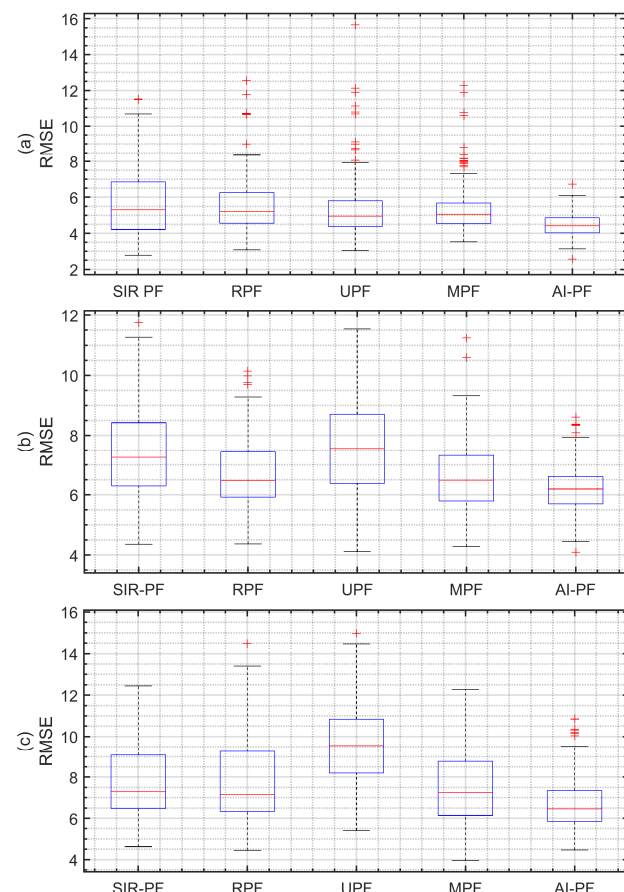


**Figure 7.** Box plots of RMSE distributions of the PF methods under different process noise variance conditions: (a)  $u = 5$ , (b)  $u = 25$ , (c)  $u = 45$ .

### (3) Computational efficiency evaluation:

To assess the computational efficiency of the related PF methods, tests are conducted to measure the execution time of each method over 200 runs. This analysis aims to evaluate the suitability of the related PF methods for real-time applications, where both processing speed and estimation accuracy are critical. In this testing, the execution time is measured in seconds (s) using MATLAB timing functions ‘tic’ and ‘toc’. Table 4 presents the average execution time for the PF methods under different particle counts over 200 simulation runs. The results indicate that the AI-PF consistently exhibits the lowest execution time under different particle count conditions. For example, with 15 particles, the AI-PF completes the execution in 0.0007 s, which is approximately 97% faster than the RPF and MPF, and 65% faster than the UPF. As the particle count increases to 75, the AI-PF maintains its efficiency with an execution time of 0.003 s, which is significantly shorter than the RPF (0.585 s), the MPF (0.593 s), and the UPF (0.008 s). The computational efficiency of the AI-PF is attributed to its proposed SDD method that selectively addresses sample degeneracy only when necessary. Additionally, the effective working mechanisms of the crossover and mutation techniques contribute by managing particle diversity within high-probability regions, which further enhance convergence. On the other hand, both the RPF and the MPF take longer execution times, which increase significantly as the particle count grows. This is because both methods employ resampling methods based on continuous distributions, leading to higher computational complexity. The UPF takes a shorter execution time compared to the RPF and MPF due to the use of unscented transformation that can prevent extensive particle propagation.

**Table 4.** Comparison of average processing time for the respective PF techniques over 200 runs.

Particle Counts	RPF (s)	UPF (s)	MPF (s)	AI-PF (s)
15	0.024	0.002	0.024	0.0007
30	0.094	0.003	0.095	0.0012
45	0.213	0.004	0.214	0.0017
60	0.372	0.006	0.379	0.0021
75	0.585	0.008	0.593	0.0030

### 3.2. Performance Evaluation for Battery RUL Prediction

In this evaluation, the proposed AI-PF is employed to predict the RUL of Li-ion batteries. The testing uses the well-accepted Li-ion battery datasets in battery prognostics research from the NASA Ames Prognostics Center [44]. Figure 8 illustrates the experimental setup, which includes Li-ion cells, chargers, electrochemical impedance spectroscopy (EIS), an environmental chamber, a load bank, sensors, a control computer, and a data acquisition system. The datasets are collected under three operational conditions (i.e., charge, discharge, impedance measurement) with constant temperature and humidity. (1) Charging: the battery is charged at 1.5 A until it reaches 4.2 V, and then it is maintained at a constant voltage until the current falls to 20 mA. (2) Discharging: the battery is discharged at 2.0 A, halting when the voltage reaches 2.5 V. (3) Impedance: EIS measurements are undertaken over a frequency range of 0.1 Hz to 5.0 kHz. The batteries are considered to have reached their end-of-life when they exhibit a 30% reduction in their rated capacity. Figure 9 shows the degradation curves for the charge capacity of four batteries from the dataset. For this test, Battery #5 is selected as the case study, which undergoes a smoothing process to reduce noise and fluctuations in the raw data so as to make the underlying trends more visible.

The effectiveness of the proposed AI-PF is assessed in this section for monitoring battery SOH and forecasting RUL. The analysis focuses on the ability to mitigate sample degeneracy in battery state estimation and modeling the battery degradation trends. The performance of AI-PF is compared with two related approaches: a quantum particle swarm optimization PF method (QPSO-PF) [36], and the mutated PF (MPF) [4]. For RUL prediction in battery SOH monitoring, battery capacity is commonly utilized as a key degradation indicator [1,4,13,18,19], which is calculated through the integration of current

over time. In this testing, the degradation behavior is represented by the model described in Equation (14), which is employed to simulate the behavior of Li-ion batteries, accounting for capacity reduction and self-recharge characteristics [3,33,34]. The capacity is subsequently transformed into the SOH using the standardized equation shown in Equation (15):

$$C_{k+1} = \eta_c C_k + b_1 \exp\left(-\frac{b_2}{\Delta t_k}\right) \quad (14)$$

$$S_{k+1} = \frac{C_{k+1}}{C_0} \times 100 \quad (15)$$

where  $\eta_c$  is the Coulombic coefficient with a value of 0.997;  $C_k$  refers to the charging capacity at the  $k$ th cycle, while  $C_0$  denotes the initial capacity when  $k = 1$ . The parameters  $b_1$  and  $b_2$  are to be estimated iteratively to capture dynamic changes in degradation trends;  $S_k$  represents the battery SOH at the  $k$ th cycle; and  $\Delta t_k$  is the resting time interval between the  $k$ th with  $(k + 1)$ th cycles, and  $\Delta t_k = 1$  in this test.

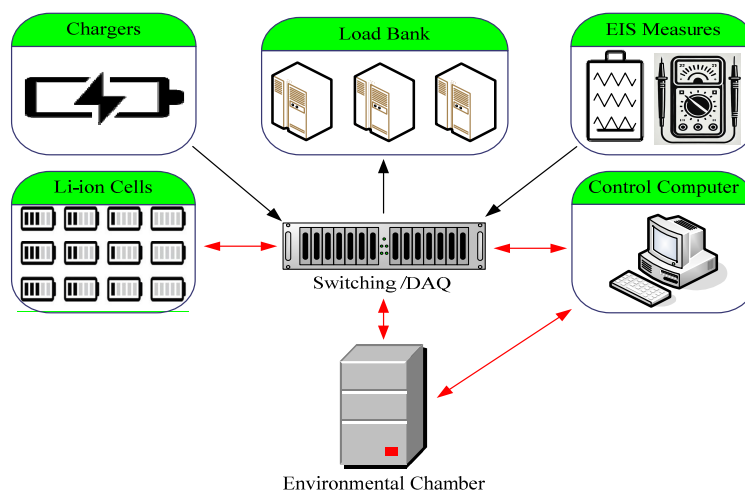


**Figure 8.** Illustration of the experimental configuration of battery tests.

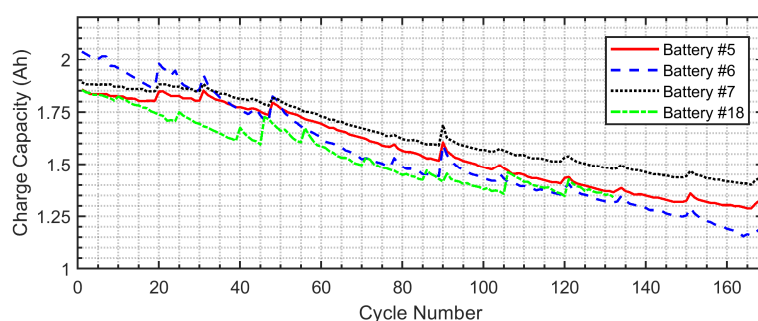


**Figure 9.** Charge capacity degradation curves for Batteries #5, #6, #7, and #18.

In this testing, 200 particles are used, which is consistent with the QPSO-PF method used in [33] to ensure comparability. The performance of the respective methods is assessed over 50 test iterations, employing data from Battery #5 in the NASA battery prognostic dataset [36], which reaches its end of life at cycle 162. Prediction start points are selected at cycles 85, 105, 125, and 145, providing representation of various battery SOH states for long-term, medium-term, and short-term predictions, and Figure 10 shows the zoomed results of the prediction starting at cycle 125. Table 5 presents the results of battery RUL predictions using the related techniques, including the absolute errors, relative errors, and the corresponding prediction initiation points.

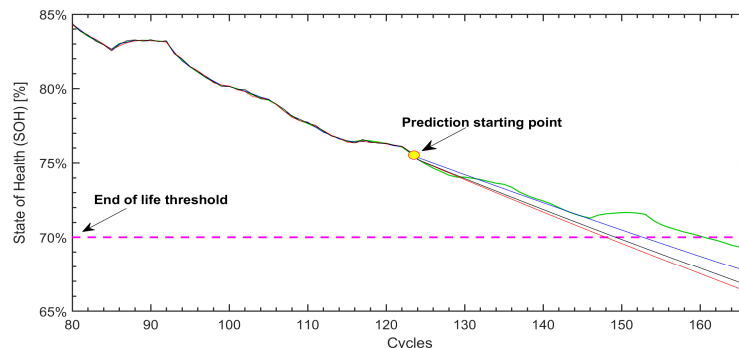


**Figure 10.** Zoomed-in performance comparison with the prediction starting at cycle 125: using MPF (red line), QPSO-PF (black line), AI-PF (blue line), and the actual states (green line).

**Table 5.** Comparison of RUL prediction results across different methods and prediction points.

Prediction Starting Point	Methods	Prediction Result (Cycle)	Absolute Error (Cycles)	Relative Error
85	MPF	141	21	12.96%
	QPSO	145	17	10.49%
	AI-PF	148	14	8.64%
105	MPF	146	16	9.88%
	QPSO	148	14	8.64%
	AI-PF	150	12	7.14%
125	MPF	148	14	8.64%
	QPSO	150	12	7.41%
	AI-PF	152	10	6.17%
145	MPF	152	10	6.17%
	QPSO	152	10	6.17%
	AI-PF	154	8	4.94%

It is seen from Table 5 that the proposed AI-PF consistently outperforms other related methods, which can achieve lower absolute and relative errors in predicting the battery RUL across various prediction starting points. For instance, at the prediction initiation point of cycle 85 (i.e., the long-term forecasting), the AI-PF achieves an absolute error of 14 cycles with a relative error of 8.64%, significantly lower than MPF 21 cycles (12.96%) and QPSO-PF 17 cycles (10.49%). This highlights the AI-PF's capability to maintain high prediction accuracy even in the early stages of battery degradation, where fluctuations in battery health are more pronounced. As the prediction initiation point moves to cycle 125 (i.e., the medium-term forecasting), the AI-PF can also achieve an absolute error of 10 cycles with a relative error of 6.17%, which outperforms MPF (14 cycles, 8.64%) and QPSO-PF (12 cycles, 7.41%) due to the adequate adaptive capability of the AI-PF. At cycle 145, which represents a later stage (i.e., short-term condition) of battery degradation, the AI-PF achieves its best performance, with an absolute error of only 8 cycles and a relative error of 4.94% compared to the errors of 10 cycles and relative errors of 6.17% of the MPF and QPSO-PF methods. The better performance of the AI-PF technique can be attributed to its adaptive sample degeneracy detection and enhanced crossover and mutation techniques, which can improve AI-PF capability in particle management, especially in high-probability regions. These mechanisms help the AI-PF effectively capture the non-linear degradation behaviors of the battery and provide more accurate SOH estimation and RUL predictions. In contrast, both MPF and QPSO-PF exhibit higher errors, particularly in the early stages of battery degradation, where they cannot adjust to rapid changes in system conditions. Although QPSO-PF shows improvement in the later stage, it still lacks the overall consistency of the AI-PF in balancing prediction accuracy at different battery SOH conditions.

The processing efficiency, measured as execution time, is a critical factor in real-time battery health monitoring and RUL prediction applications. Table 6 and Figures 11–13

present the average execution time of MPF, QPSO-PF, and the proposed AI-PF methods, evaluated over 50 random runs at different prediction starting points. It is clear that the QPSO-PF exhibits the longest execution time due to its iterative optimization process and the wave function-based particle duplication operation, which significantly increases computational complexity. In contrast, MPF demonstrates moderate execution time by balancing computational efficiency and robustness without the overhead of excessive optimization. However, the proposed AI-PF can achieve shorter execution time than both QPSO-PF and MPF. For instance, at cycle 145, the proposed AI-PF completes its computations in just 0.0064 s, whereas QPSO-PF and MPF require 4.026 s and 0.0184 s, respectively. The high computation efficiency of the proposed AI-PF is attributed to its innovative SDD mechanism, which selectively addresses sample degeneracy only, thereby reducing computation complexity. Furthermore, its crossover and mutation approaches can enhance particle diversity in high-probability regions, which can improve convergence. These results highlight that the proposed AI-PF has potential for real-time battery monitoring applications.

**Table 6.** Execution time comparison (average over 50 runs) for RUL prediction across various starting points.

Prediction Starting Point	Methods	Time (s)
85	MPF	0.0124
	QPSO-PF	2.1299
	AI-PF	0.0037
105	MPF	0.0142
	QPSO-PF	2.6447
	AI-PF	0.0047
125	MPF	0.0162
	QPSO-PF	3.1640
	AI-PF	0.0056
145	MPF	0.0184
	QPSO-PF	4.0260
	AI-PF	0.0064

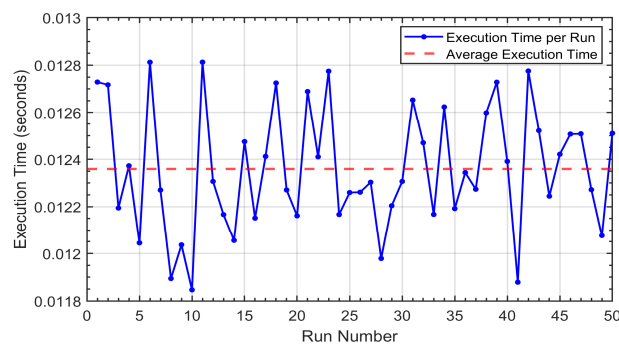


**Figure 11.** Execution times for MPF at the prediction starting point of cycle 85 over 50 runs.

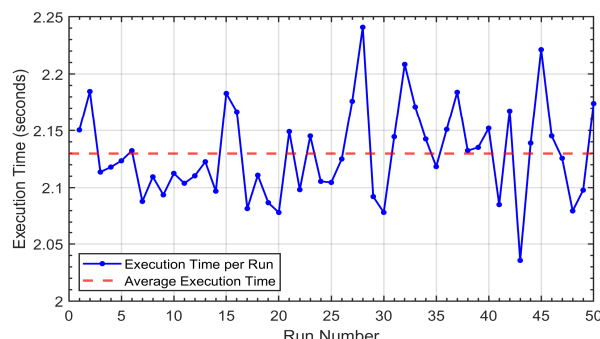


**Figure 12.** Execution times for QPSO-PF at the prediction starting point of cycle 85 over 50 runs.

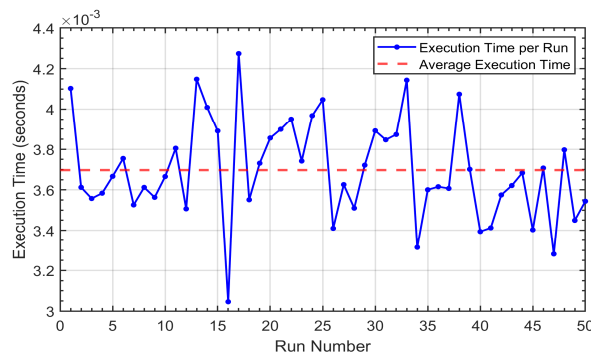


**Figure 13.** Execution times for AI-PF at the prediction starting point of cycle 85 over 50 runs.

#### 4. Conclusions

This paper presents a novel AI-driven particle filter technique, AI-PF, designed to enhance battery SOH monitoring and RUL prediction. The AI-PF technique aims to mitigate the critical issues in PF methods such as sample degeneracy and particle impoverishment. A dynamic sample degeneracy detection method is proposed to selectively identify and mitigate degeneracy only when necessary so as to improve computational efficiency. Enhanced crossover and mutation techniques are suggested to adaptively adjust particle locations on high-probability regions and maintain particle diversity so as to further enhance convergence and accuracy. The effectiveness of the proposed AI-PF has been validated through extensive simulation tests using the related benchmark models and battery test datasets. The results demonstrate that the AI-PF can effectively reduce sample degeneracy and particle impoverishment. It can reduce up to 33% of RMSE and significantly reduce computational time in comparison with the related PF methods. Moreover, the AI-PF has adequate adaptive capability to improve SOH estimation and RUL prediction across different prediction starting points. It also achieves significant improvements in RUL prediction accuracy, with relative errors as low as 4.94%, and the lowest execution times compared to other PF methods. It has a potential to be applied for real-time battery health monitoring and prognostic applications.

While the proposed AI-PF demonstrates significant advancements, advanced research is undertaken to address its possible limitations: (1) sensitivity to hyperparameter tuning under varying system conditions, (2) scalability for high-dimensional systems and real-time implementation, and (3) the effect of initial state selection. Additionally, advanced research and development have been undertaken to further improve the PF methods to update the posterior PDF during the prognostic phase when new measurement data are unavailable. The purpose is to further improve the adaptive capability of the proposed AI-PF technique in real-world applications.

**Author Contributions:** Conceptualization, M.A.; methodology, M.A. and W.W.; validation, M.A. and W.W.; formal analysis, M.A. and W.W.; investigation, M.A. and W.W.; resources, W.W.; data curation, M.A.; writing—original draft preparation, M.A.; writing—review and editing, M.A. and W.W.; supervision, W.W.; funding acquisition, W.W. All authors have read and agreed to the published version of the manuscript.

**Funding:** This research received no external funding.

**Data Availability Statement:** The data that support the findings of this study are openly available in: NASA dataset: Prognostics Center of Excellence Data Set Repository at <https://phm-datasets.s3.amazonaws.com/NASA/5.+Battery+Data+Set.zip> (accessed on 1 May 2024).

**Acknowledgments:** This project was partially supported by the Natural Sciences and Engineering Research Council of Canada (NSERC), eMech Systems Inc., and Bare Point Water Treatment Plant in Thunder Bay, ON, Canada.

**Conflicts of Interest:** The authors declare no conflicts of interest.

## References

1. Ge, M.-F.; Liu, Y.; Jiang, X.; Liu, J. A review on state of health estimations and remaining useful life prognostics of lithium-ion batteries. *Measurement* **2021**, *174*, 109057. [[CrossRef](#)]
2. Wang, J.; Meng, J.; Peng, Q.; Liu, T.; Zeng, X.; Chen, G.; Li, Y. Lithium-ion battery state-of-charge estimation using electrochemical model with sensitive parameters adjustment. *Batteries* **2023**, *9*, 180. [[CrossRef](#)]
3. Pola, D.A.; Navarrete, H.F.; Orchard, M.E.; Rabie, R.S.; Cerdá, M.A.; Olivares, B.E.; Silva, J.F.; Espinoza, P.A.; Perez, A. Particle-filtering-based discharge time prognosis for lithium-ion batteries with a statistical characterization of use profiles. *IEEE Trans. Reliab.* **2015**, *64*, 710–720. [[CrossRef](#)]
4. Li, D.Z.; Wang, W.; Ismail, F. A mutated particle filter technique for system state estimation and battery life prediction. *IEEE Trans. Instrum. Meas.* **2014**, *63*, 2034–2043. [[CrossRef](#)]
5. Kordestani, M.; Saif, M.; Orchard, M.E.; Razavi-Far, R.; Khorasani, K. Failure prognosis and applications—A survey of recent literature. *IEEE Trans. Reliab.* **2019**, *70*, 728–748. [[CrossRef](#)]
6. Wang, D.; Miao, Q.; Pecht, M. Prognostics of lithium-ion batteries based on relevance vectors and a conditional three-parameter capacity degradation model. *J. Power Sources* **2013**, *239*, 253–264. [[CrossRef](#)]
7. Nuhic, A.; Terzimehic, T.; Soczka-Guth, T.; Buchholz, M.; Dietmayer, K. Health diagnosis and remaining useful life prognostics of lithium-ion batteries using data-driven methods. *J. Power Sources* **2013**, *239*, 680–688. [[CrossRef](#)]
8. Yang, D.; Wang, Y.; Pan, R.; Chen, R.; Chen, Z. A neural network based state-of-health estimation of lithium-ion battery in electric vehicles. *Energy Procedia* **2017**, *105*, 2059–2064. [[CrossRef](#)]
9. Dai, H.; Guo, P.; Wei, X.; Sun, Z.; Wang, J. ANFIS based online SOC (State of Charge) correction considering cell divergence for the EV (electric vehicle) traction batteries. *Energy* **2015**, *80*, 350–360. [[CrossRef](#)]
10. Chen, M.; Ma, G.; Liu, W.; Zeng, N.; Luo, X. An overview of data-driven battery health estimation technology for battery management system. *Neurocomputing* **2023**, *532*, 152–169. [[CrossRef](#)]
11. Zhang, J.; Lee, J. A review on prognostics and health monitoring of Li-ion battery. *J. Power Sources* **2011**, *196*, 6007–6014. [[CrossRef](#)]
12. Skrjanc, I.; Iglesias, J.; Sanchis, A.; Leite, D.; Lughofer, E.; Gomide, F. Evolving fuzzy and neuro-fuzzy approaches in clustering, regression, identification, and classification: A survey. *Inf. Sci.* **2019**, *490*, 344–368. [[CrossRef](#)]
13. Hu, X.; Xu, L.; Lin, X.; Pecht, M. Battery lifetime prognostics. *Joule* **2020**, *4*, 310–346. [[CrossRef](#)]
14. El Mejdoubi, A.; Chaoui, H.; Gualous, H.; Bossche, P.V.D.; Omar, N.; Van Mierlo, J. Lithium-ion batteries health prognosis considering aging conditions. *IEEE Trans. Power Electron.* **2018**, *34*, 6834–6844. [[CrossRef](#)]
15. Ahwiadi, M.; Wang, W. An enhanced mutated particle filter technique for system state estimation and battery life prediction. *IEEE Trans. Instrum. Meas.* **2018**, *68*, 923–935. [[CrossRef](#)]
16. Simon, D. *Optimal State Estimation: Kalman, Nonlinear Approaches*; Wiley Publisher: Hoboken, NJ, USA, 2006.
17. Arulampalam, M.; Maskell, S.; Gordon, N.; Clapp, T. A tutorial on particle filters for online nonlinear/non-Gaussian Bayesian tracking. *IEEE Trans. Signal Process.* **2002**, *50*, 174–188. [[CrossRef](#)]
18. Saha, B.; Goebel, K.; Poll, S.; Christoffersen, J. An integrated approach to battery health monitoring using Bayesian regression and state estimation. In Proceedings of the 2007 IEEE Autotestcon, Baltimore, MD, USA, 17–20 September 2007; pp. 646–653.
19. Saha, B.; Goebel, K. Modeling Li-ion battery capacity depletion in a particle filtering framework. In Proceedings of the Annual Conference of the Prognostics and Health Management Society, San Diego, CA, USA, 27 September–1 October 2009; pp. 1–10.
20. Walker, E.; Rayman, S.; White, R.E. Comparison of a particle filter and other state estimation methods for prognostics of lithium-ion batteries. *J. Power Sources* **2015**, *287*, 1–12. [[CrossRef](#)]
21. Dong, G.; Chen, Z.; Wei, J.; Ling, Q. Battery health prognosis using Brownian motion modeling and particle filtering. *IEEE Trans. Ind. Electron.* **2018**, *65*, 8646–8655. [[CrossRef](#)]
22. Wang, D.; Yang, F.; Zhao, Y.; Tsui, K.-L. Battery Remaining Useful Life Prediction at Different Discharge Rates. *Microelectron. Reliab.* **2017**, *78*, 212–219. [[CrossRef](#)]
23. Li, T.; Sun, S.; Sattar, T.P.; Corchado, J.M. Fight sample degeneracy and impoverishment in particle filters: A review of intelligent approaches. *Expert Syst. Appl.* **2014**, *41*, 3944–3954. [[CrossRef](#)]
24. Ahwiadi, M.; Wang, W. An enhanced particle filter technology for battery system state estimation and RUL prediction. *Measurement* **2022**, *191*, 110817. [[CrossRef](#)]
25. Kotecha, J.H.; Djuric, P.M. Gaussian particle filtering. *IEEE Trans. Signal Process.* **2003**, *51*, 2592–2601. [[CrossRef](#)]
26. Haque, M.S.; Choi, S.; Baek, J. Auxiliary particle filtering-based estimation of remaining useful life of IGBT. *IEEE Trans. Ind. Electron.* **2018**, *65*, 2693–2703. [[CrossRef](#)]
27. Miao, Q.; Xie, L.; Cui, H.; Liang, W.; Pecht, M. Remaining useful life prediction of lithium-ion battery with unscented particle filter technique. *Microelectron. Reliab.* **2013**, *53*, 805–810. [[CrossRef](#)]
28. Wang, D.; Yang, F.; Tsui, K.-L.; Zhou, Q.; Bae, S.J. Remaining useful life prediction of lithium-ion batteries based on spherical cubature particle filter. *IEEE Trans. Instrum. Meas.* **2016**, *65*, 1282–1291. [[CrossRef](#)]
29. Musso, C.; Oudjane, N.; LeGland, F. Improving Regularized Particle Filters. In *Sequential Monte Carlo Methods in Practice*; Springer: New York, NY, USA, 2001.
30. Liu, J.; Wang, W.; Ma, F. A regularized auxiliary particle filtering approach for system state estimation and battery life prediction. *Smart Mater. Struct.* **2011**, *20*, 075021. [[CrossRef](#)]

31. Lin, Y.-H.; Jiao, X.-L. Adaptive kernel auxiliary particle filter method for degradation state estimation. *Reliab. Eng. Syst. Saf.* **2021**, *211*, 107562. [[CrossRef](#)]
32. Murangira, A.; Musso, C.; Dahia, K. A mixture regularized rao-blackwellized particle filter for terrain positioning. *IEEE Trans. Aerosp. Electron. Syst.* **2016**, *52*, 1967–1985. [[CrossRef](#)]
33. Yin, S.; Zhu, X. Intelligent particle filter and its application on fault detection of nonlinear system. *IEEE Trans. Ind. Electron.* **2015**, *62*, 3852–3861. [[CrossRef](#)]
34. Yu, M.; Li, H.; Jiang, W.; Wang, H.; Jiang, C. Fault diagnosis and rul prediction of nonlinear mechatronic system via adaptive genetic algorithm-particle filter. *IEEE Access* **2019**, *7*, 11140–11151. [[CrossRef](#)]
35. Tian, Y.; Lu, C.; Wang, Z.; Tao, L. Artificial Fish Swarm Algorithm-Based Particle Filter for Li-Ion Battery Life Prediction. *Math. Probl. Eng.* **2014**, *2014*, 1–10. [[CrossRef](#)]
36. Yu, J.; Mo, B.; Tang, D.; Liu, H.; Wan, J. Remaining Useful Life Prediction for Lithium-Ion Batteries Using a Quantum Particle Swarm Optimization-Based Particle Filter. *Qual. Eng.* **2017**, *29*, 536–546. [[CrossRef](#)]
37. Ouyang, T.; Ye, J.; Xu, P.; Wang, C.; Xu, E. Estimation of state-of-charge and state-of-health for lithium-ion battery based on improved firefly optimized particle filter. *J. Energy Storage* **2023**, *68*, 107733. [[CrossRef](#)]
38. Zhang, C.; Zhu, Y.; Dong, G.; Wei, J. Data-driven lithium-ion battery states estimation using neural networks and particle filtering. *Int. J. Energy Res.* **2019**, *43*, 8230–8241. [[CrossRef](#)]
39. Sbarufatti, C.; Corbetta, M.; Giglio, M.; Cadini, F. Adaptive prognosis of lithium-ion batteries based on the combination of particle filters and radial basis function neural networks. *J. Power Sources* **2017**, *344*, 128–140. [[CrossRef](#)]
40. Wang, X.-L.; Li, L.-Q.; Xie, W.-X. A novel T-S fuzzy particle filtering algorithm based on fuzzy C-regression clustering. *Int. J. Approx. Reason.* **2020**, *117*, 81–95. [[CrossRef](#)]
41. Zhao, J.; Liu, M.; Zhang, B.; Wang, X.; Liu, D.; Wang, J.; Bai, P.; Liu, C.; Sun, Y.; Zhu, Y. Review of lithium-ion battery fault features, diagnosis methods, and diagnosis procedures. *IEEE Internet Things J.* **2023**, *11*, 18936–18950. [[CrossRef](#)]
42. Lipu, M.H.; Hannan, M.; Hussain, A.; Hoque, M.; Ker, P.J.; Saad, M.; Ayob, A. A review of state of health and remaining useful life estimation methods for lithium-ion battery in electric vehicles: Challenges and recommendations. *J. Clean. Prod.* **2018**, *205*, 115–133. [[CrossRef](#)]
43. Tian, H.; Qin, P.; Li, K.; Zhao, Z. A review of the state of health for lithium-ion batteries: Research status and suggestions. *J. Clean. Prod.* **2020**, *261*, 120813. [[CrossRef](#)]
44. Saha, B.; Goebel, K. “Battery Data Set”, NASA Prognostics Data Repository, NASA Ames Research Center, Moffett Field, CA, USA. Available online: <https://phm-datasets.s3.amazonaws.com/NASA/5.+Battery+Data+Set.zip> (accessed on 1 May 2024).

**Disclaimer/Publisher’s Note:** The statements, opinions and data contained in all publications are solely those of the individual author(s) and contributor(s) and not of MDPI and/or the editor(s). MDPI and/or the editor(s) disclaim responsibility for any injury to people or property resulting from any ideas, methods, instructions or products referred to in the content.